Journal of Food Bioactives
International Society for Nutraceuticals and Functional Foods
Original Research
J. Food Bioact. 2023;23:19–34

Anthocyanins-rich purple potato extract prevents low-grade chronic inflammation-associated metabolic disorders

Hua Zhang[a], Ronghua Liu[a], Lili Mats[a], Dion Lepp[a], Honghui Zhu[a], Yuhuan Chen[a], Shilian Zheng[a], Yoshinori Mine[b] and Rong Tsao[a*]

[a]Guelph Research & Development Centre, Agriculture and Agri-Food Canada, 93 Stone Road West, Guelph, Ontario, Canada, N1G 5C9
[b]Food Science Department, University of Guelph, 50 Stone Road East, Guelph, Ontario, Canada, N1G 2W1
[*]**Corresponding author:** Rong Tsao, Guelph Research & Development Centre, Agriculture and Agri-Food Canada, 93 Stone Road West, Guelph, Ontario, Canada, N1G 5C9. Tel. +1 226 217 8180; Fax: +1 226 217 8183; E-mail: Rong.Cao@agr.gc.ca
DOI: 10.31665/JFB.2023.18351
Received: June 11, 2023; **Revised received & accepted:** June 29, 2023
Citation: Zhang, H., Liu, R., Mats, L., Lepp, D., Zhu, H., Chen, Y., Zheng, S., Mine, Y., and Tsao, R. (2023). Anthocyanins-rich purple potato extract prevents low-grade chronic inflammation-associated metabolic disorders. J. Food Bioact. 23: 19–34.

Abstract

Dietary polyphenols including anthocyanins possess strong antioxidant and anti-inflammatory properties, and are known to help reduce risks of oxidative stress-induced chronic diseases. However, their effects on various aspects of the gut microenvironment towards preventing the unhealthy diet-induced metabolic disorders are still not well understood. The present study aims to verify the in vitro antioxidant and anti-inflammatory effects of the anthocyanin-rich extracts of purple potato (PPE), using a lipopolysaccharide (LPS) and high-fat diet (HFD)-induced obesity C57/BL6J mouse model, and to examine the effects of PPE on LPS+HFD-impaired metabolic homeostasis and the underlying mechanisms. We found that PPE, especially at higher dose significantly improved the glucose and lipid metabolism, and reduced inflammation in the plasma and various tissues. It significantly improved intestinal barrier integrity, altered fecal metabolite profile and gut microbiota composition. Our findings provide new insights into the roles of highly-pigmented vegetable-derived anthocyanins in maintaining gut health and ameliorating metabolic syndrome.

Keywords: Anthocyanin; Purple potato; High-fat diet; Low-grade inflammation; Metabolism; Intestinal barrier integrity; Gut microbiota; Metabolic syndrome.

1. Introduction

Diet is a key epigenetic factor that affects overall human health. Diet high in fat is typically unhealthy and can negatively impact on gut microbiota diversity and intestinal integrity (Alcock et al., 2014; Tang et al., 2019). Shifts in gut microbiota composition triggered by high fat diet (HFD) and direct actions from the colonic metabolites such as the short chain fatty acids (SCFA) on intestinal cells are the first step towards the development and mediation of chronic systemic inflammation (Duan et al., 2018). Alterations in gut microbiota populations can also activate Toll-like receptor (TLR) signaling pathways, leading to increased intestinal permeability to bacterial components such as lipopolysaccharides (LPS). LPS can enter into the submucosal layer of the human digestive tract to induce mucosal inflammation, which causes the gut to lose mucosal immune homeostasis, leading to macrophage polarization into the activated macrophage M1. These activated M1 can trigger innate immune responses by elevating pro-inflammatory mediators, promoting the translocation of LPS into circulation (Duan et al., 2018). Endotoxins in the circulation system results in metabolic endotoxemia, eliciting a chronic low-grade pro-inflammatory and pro-oxidative stress status that increases the risk of developing metabolic syndrome and chronic diseases such as type II diabetes, cardiovascular diseases, non-alcoholic fatty liver diseases and others (Moreira et al., 2012). A growing body of evidence supports a role for diet in overall health and points to the fact that the loss of

mucosal barrier integrity may initiate the progress of developing chronic inflammatory tone in the entire body (Castillo-Armengol et al., 2019; Pendyala et al., 2012; Tang et al., 2019). This systemic low-grade chronic inflammation has a profound negative impact on the control of immune and metabolic homeostasis, leading to dysregulation and disease susceptibility (Kotas and Medzhitov, 2015). Therefore, changes to nutritional or dietary components can induce epigenetic modifications associated with the metabolic and immune balance.

The gut barrier is a primary line of defense in protecting the complex internal body system from direct exposure to harmful stimulus (e.g. pathogens, toxins and viruses), symbiotic microbiome, microbial metabolites and other exogenous substances from the diet (Halfvarson et al., 2017). The human intestinal membrane represents a complex system consisting of the epithelial layer, lymphatic tissues and blood vessel for the absorption and delivery of nutrients. More importantly, the intestinal lumen also provides a niche to harbor symbiotic microbiota that are involved in shaping mucosal immune responses (Garrett et al., 2010). Hence, an intact intestinal lumen plays a key role in maintaining the balance between commensal bacteria and immune tolerance. However, the loss of gut barrier integrity impairs the homeostasis in the gut microenvironment by which commensal bacteria can induce a persistent innate immune response. Chronic exposure to LPS elicits gut inflammation by activating TLR-4 of the intestinal epithelial cells, leading to dysbiosis of gut microbiota, permanent damage of intestinal tissues and dysfunction of the gut (Heyman-Linden et al., 2016; Zeng et al., 2019). The leaky gut in turn results in the influx of luminal virulent substances, including pathobiont and LPS, into the circulatory system that provokes metabolic endotoxemia, which leads to insulin resistance and increased susceptibility to diabetes mellitus (Gomes et al., 2017).

Anthocyanins are natural purple pigments that exist widely in fruits and vegetables (Joseph et al., 2014). Many studies have shown solid evidence of the health benefits of anthocyanin-rich foods. Anthocyanins are involved in the regulation of signal transduction pathways to inhibit inflammatory responses at a cellular level, thereby lowering the risk of developing inflammatory diseases (Nunez and Magnuson, 2013; Tsuda, 2012; Vendrame and Klimis-Zacas, 2015). The majority of studies focus on the anti-inflammatory properties of fruit-derived anthocyanins rather than that of vegetables. However, the phenotypic and functional properties of anthocyanins derived from different plant resources can directly affect the efficacy of their health promoting properties. Highly pigmented root vegetables such as purple coloured potatoes and carrots are important dietary sources of anthocyanins and fibers, and may be more advantageous than small berry fruits as a diet source when it comes to cost and shelf-life. Previously, we reported that anthocyanin-rich extracts derived from these highly pigmented root vegetables significantly suppressed LPS-induced inflammatory signal transduction in submucosal macrophages after being absorbed in a co-culture cell model (Hua Zhang et al., 2017). The study also showed that purple potato extract (PPE) rich in petunidin glycoside had a higher bioavailability compared with that of purple carrots rich in cyanidin glycoside. The preferred bioavailability of petunidin glycoside was partially due to its affinity for the glucose transporter and increased stability under neutral pH by the methoxyl group (Fossen et al., 1998; Khoo et al., 2017; Wahlström et al., 2016; Hua Zhang et al., 2017). However, it is not known if the purple potato derived anthocyanins exert similar anti-inflammatory effects *in vivo* and have a preventative effect on metabolic dysfunctions through the core of gut.

The regulatory attributes of dietary substances, particularly food-derived bioactives such as anthocyanins, may counter the negative impact of unhealthy constituents in the gut, where there exists an intimate relationship between the immune system and colonic metabolism. Food bioactives may also be involved in modulating epigenetic markers throughout the whole body (Alcock et al., 2014; Tang et al., 2019). How dietary polyphenols including anthocyanins modulate the various aspects of the gut microenvironment towards preventing the unhealthy diet-induced metabolic disorders is still not well understood. The present study therefore aims to determine the effects of purple potato extract on endotoxemia-impaired metabolic homeostasis and to investigate the underlying mechanisms using an LPS- and HFD-induced obesity mouse model. Findings of the present study will provide new insights into the contextual dependency of the effects of highly-pigmented root vegetable-derived anthocyanins on gut health and disease susceptibility.

2. Materials and methods

2.1. Chemicals and reagents

Low-grade chronic inflammation was induced by LPS isolated from *Escherichia coli* (*E. coli*) 0111: B4 (Sigma, Oakville, Ontario, Canada). D-Mannitol and fluorescein isothiocyanate-dextran (FD4) (Sigma) were used to detect gut leaking. Plasma D-mannitol concentration was measured by D-mannitol assay kit (Colorimetric) (Abcam Inc. Toronto, Ontario, Canada). Glucose (Sigma) was used for glucose tolerance test (GTT). Plasma insulin was measured by ultra-sensitive mouse insulin ELISA kit (Crystal Chem, Elk Grove Village, IL, USA). Plasma endotoxin concentration was measured by Pierce LAL chromogenic endotoxin quantitation kit (Thermo Scientific, Whitby, Ontario, Canada). Cytokines, TNF-α, MCP-1, and IL-10 were measured using Ready-SET-Go! ELISA kits by following each supplier's instruction (eBioscience, Affymetrix, Inc. San Diego, CA, USA). Adiponectin was measured by mouse adiponectin/Acrp30 Duo-Set ELISA (R&D Systems, Minneapolis, MN, USA). Plasma total cholesterol, high-density lipoprotein (HDL), and low-density lipoprotein (LDL) cholesterol were measured by cholesterol assay kit - HDL and LDL/VLDL (Abcam Inc.). Plasma LPS binding protein (LBP) was measured by LBP, mouse, ELISA kit (Hycult Biotech Inc. Wayne, USA). Radioimmunoprecipitation assay (RIPA) buffer (Thermo Scientific), protease inhibitor cocktail (Thermo Scientific), and phenylmethanesulfonyl fluoride (PMSF) (Sigma) were used for white adipose tissues, jejunum, and colon protein extraction. The following antibodies were used for Western blot (WB) of white adipose tissue homogenate: Peroxisome proliferator-activated receptor gamma (PPAR-γ) antibody (Cell Signaling, Dancers, MA, USA), insulin receptor substrate 1 (IRS-1) antibody (Cell Signaling), β-actin rabbit mAb (HRP conjugate) (Cell Signaling), HRP conjugated anti-rabbit IgG (Promega, Madison, WI, USA). Amersham ECL prime western blotting detection reagent (GE Healthcare, Mississauga, Ontario, Canada) was used for WB detection. F4/80 antibody (Santa Cruz Biotechnology, Mississauga, Ontario, Canada) was used for immunohistochemistry of white adipose tissues.

2.2. Experimental design

The animal study was approved by the University of Guelph Animal Care Committee and followed in accordance with the Canadian Council on Animal Care Guide to the Care and Use of Experimental Animals. The Animal Utilization Protocol (AUP) number of this animal study is AUP3502. All mice were housed in the Cen-

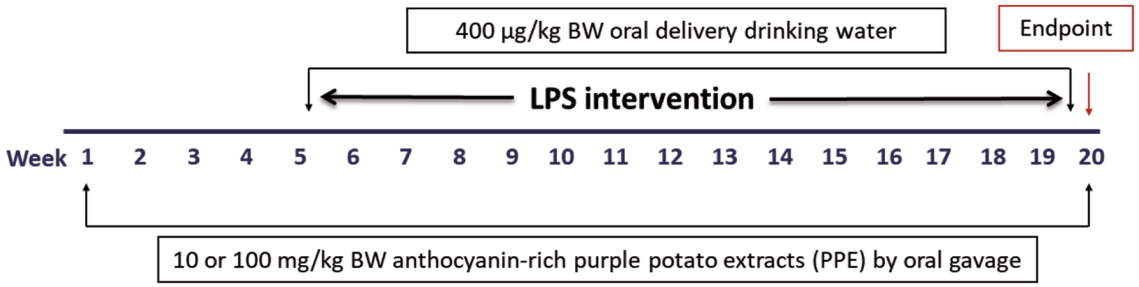

Figure 1. Schematic diagram of the animal experiment. C57BL/6J female mice were randomly assigned to the groups. Normal diet was 10% fat (as a percentage of total kcal) and high-fat diet was 60% fat (as a percentage of total kcal). PPE was supplemented to mice by oral gavage. NC: negative control group 1, HFD/LPS: positive control group, LPP: low-dose PPE treated group, HPP: high-dose PPE treated group. Each group had 12 mice (n = 12).

tral Animal Facility (CAF) at the University of Guelph (Guelph, ON) during the animal trial. Sixty female C57BL/6J mice (15–16 weeks, 18–22 g; Charles River Laboratories, Montreal, QC) were housed at 22–25 °C, 55±15% humidity and 12 h light/dark cycle with unrestrained access of food and water. The high fat diet (HFD) (formula TD.06414) and normal diet (formula TD.94045) applied in this study were prepared by ENVIGO (Madison, WI, USA), and the composition is listed in Table S1. There are 5 groups in this study as listed below and each group included 12 mice: control groups (negative control (NC) group, HFD-treated group (HF), HFD and LPS-treated group (HF/LPS)) and two purple potato extracts (PPE) intervention groups (low-dose PPE (LPP) at 10 mg/kg BW and high-dose PPE (HPP) at 100 mg/kg BW) as shown in Figure 1. The doses were selected based on existing literature data on mouse and human trials (Hurst et al., 2020; Nair and Jacob, 2016; Nemes et al., 2019). During the entire 20 week trial, mice in NC received autoclaved water and 10% fat (percentage of total kcal) mouse diet. Except for mice of NC, all mice in this trial were administered a HFD from week 5. In addition, mice of HF/LPS, LPP and HPP groups were treated with 400 μg/kg BW of LPS through drinking water from week 5. Both low-dose (10 mg/kg BW) and high-dose (100 mg/kg BW) PPE were supplemented with treatment groups 3 times/week by oral gavage throughout the entire trial. After carrying out a glucose tolerance or a gut permeability test at week 20, the animals were humanely euthanized using CO_2 asphyxiation. Blood was then immediately collected by cardiac puncture in EDTA-coated tubes, and then centrifuged at 2,500 ×*g*, 4 °C for 20 min to collect plasma into 2 mL screwcap microtubes for ELISA assays. Abdominal white adipose tissues, jejunum, and colon were also collected, and either stored in 10% formalin for immunohistochemical analysis or stored at −80 °C for Western blot and real-time PCR (RT-PCR) analyses.

2.3. Glucose tolerance test

GTT was performed in 6 mice per group at the endpoint. The results of a GTT were used as an index to determine the onset of insulin resistance. Mice were fasted precisely 6 hours prior to the test. A drop of blood was collected from the cutting of the mouse tail and applied onto a glucose meter (ONETOUCH Ultra, Burnaby, British Columbia, Canada). Blood glucose levels determined at that point were recorded as baseline levels. Each mouse was then introduced by oral gavage a 150 μL bolus of glucose (2 g/kg body weight, Sigma) in autoclaved water. Glucose levels were subsequently measured and recorded at 15, 30, 60, and 120 min post-glucose administration. Data were calculated as area under the curve (AUC) within the 120 min.

2.4. Intestinal permeability assessment

Intestinal permeability test was performed by oral gavage of D-mannitol (Sigma-Aldrich) in 6 mice per group. Mice were fasted precisely 6 h prior to the test. Each mouse was administered by oral gavage a bolus of 150 μL D-mannitol (0.6 g/kg body weight, Sigma) dissolved in autoclaved water. Mice were then refrained from water and food for 2 h before being euthanized by CO_2 asphyxiation. Blood was collected as in aforementioned procedure for ELISA assays. The plasma concentrations of D-mannitol were measured using a colorimetric assay kit and recorded as an intestinal permeability index.

2.5. Enzyme-linked immunosorbent assays

The concentrations of TNF-α, MCP-1 and adiponectin in plasma were measured using Ready-SET-Go!™ ELISA kits (eBiosciences) according to the manufacturer's instructions. ELISA plates (96-well) (Corning, Corning, NY, USA) were coated overnight at 4 °C with 100 μL per well of capture antibody in coating buffer. Plates then were washed with 0.1 M phosphate-buffered saline (PBS), pH 7.4, containing 0.05% Tween 20 (PBST) using the BioTek microplate washer (BioTek, Winooski, VT). Each well was then blocked with 200 μL 1X ELISA diluent at 37 °C for 1 h on an orbital shaker. Standards for each respective ELISA assay were serially diluted according to the manufacturer's instructions. After washing with PBST, a volume of 100 μL/well of diluted plasma (1:2 or 1:4 v/v) or 100 μL of standards was added to the plate and incubated for 2 h at 37 °C. Following this, 100 μL per well of avidin horseradish peroxidase (Avidin-HRP) was added and incubated at 37 °C for 30 min with gentle shaking. Detection was carried out using 100 μL per well of avidin-horseradish peroxidase conjugate and TMB substrate (Sigma-Aldrich). The reaction was stopped using 50 μL per well of 0.5 N H_2SO_4, and absorbance was measured at 450 nm using a microplate reader (iMark model 550, Bio-Rad). Plasma TNF-α, MCP-1 and adiponectin concentrations were determined from the standard calibration curves and quantified as pg/mL in plasma.

2.6. Western blot

Approximately 300 mg of white adipose tissues (WAT) was lysed in 300 μL ice-cold radio-immunoprecipitation assay (RIPA) buffer (Thermo Fisher) containing Halt™ Protease and Phosphatase Inhibitor Cocktail (Thermo Fisher), and then homogenized using bead mill homogenizer (Fisher Scientific). The supernatant was

collected after centrifuging at 2,500 ×*g*, 4 °C for 30 min. Protein concentration was measured using the DC Protein Assay (Bio-Rad). Western blot analysis was carried out using the following procedure as previously described with slight modifications (Zhang et al., 2015). Total protein samples were resolved by SDS-PAGE (10%) and transferred onto a nitrocellulose membrane (Bio-Rad). Membranes were blocked using 25 mL of 5% non-fat milk powder in Tris-buffered saline (TBS), and incubated with 10 mL primary antibody at a dilution of 1:2,000 (v/v) overnight at 4 °C. Detection was carried out using 10 mL of HRP-conjugated anti-mouse or anti-rabbit IgG (Promega, Madison, MI, USA) at the dilution rate of 1:10,000 (v/v) and ECL Western Blotting Detection Reagent (GE Healthcare, Mississauga, ON, Canada). Densitometry was performed using Image J software (Image Processing and Analysis in Java, National Institutes of Health, http://rsbweb.nih.gov/ij/).

2.7. Immunohistochemical analysis

The WAT were dissected, fixed and stored in 10% (w/v) buffered formalin and embedded into paraffin. The embedded sections of WAT were then performed as previously described (Zhang et al, 2020). Briefly, the de-paraffined samples were immersed into pre-heated antigen retrieval buffer for 10 min at 95 °C. Samples were then washed in PBS three times, 5 min per wash. The samples were blocked with 5% bovine serum albumen (BSA) in PBST for 30 min at 37 °C, and then incubated with F4/80 antibody (Santa Cruz Biotechnology) diluted (1:1,000 (v/v)) in 5% BSA in PBST for 1 h at room temperature. After washing, samples were then incubated with secondary antibody diluted (1:1,000 (v/v)) in 5% BS) in PBST for 1 h at room temperature, followed by 3x washes in PBS. 3,3′-Diaminobenzidine (DAB) was used to stain the samples. Hematoxylin was used for counterstaining and mounting was performed using nail polish (Crosby, 2016). The slides were subsequently examined by light microscopy (Olympus Life Sciences). The total number of adipocytes vs. number of adipocytes with crown-like structure showing macrophage infiltration were counted. The percentage of adipocytes with macrophage infiltration was calculated.

2.8. RNA isolation and RT-PCR

Total RNA was extracted from jejunum and colon tissues using the PerfectPure RNA Cultured Cell Kit (5 Prime, Gaithersburg, MD, USA) according to the manufacturer's instructions. One microgram of total RNA was reverse transcribed into cDNA using a qScript™ cDNA Synthesis Kit (Quanta Biosciences, Inc., Gaithersburg, MD). RT-PCR was carried out using iQ SYBR Green Supermix (Quanta Biosciences) on Applied Biosystem 7500 Fast and 7500 RT-PCR system (Thermo Fisher Scientific) using the following conditions: 45 cycles of denaturation at 95 °C for 15 s, annealing and extension at 60 °C for 1 min using the primers listed in previous publication (Zhang et al., 2016). Relative gene expression was calculated using the 2-ΔΔCt method using GAPDH as the reference gene (Livak and Schmittgen, 2001). Results were presented as fold expression change relative to the negative control representing untreated samples.

2.9. Fecal metabolite profile

2.9.1. Fecal short chain fatty acid (SCFA) profile

Mouse fecal pellets were freshly collected by individually housing the mice in a container at various time points i.e. pre-treatment, halfway point and at the endpoint of the study, and then freeze-dried in a bulk tray dryer Freezone 12 (Labconco, Kansas City, MO, USA). The freeze-dried fecal samples were homogenized in 30% (v/w) of ultra-pure water (Thermo Scientific), and then extracted with 70% (v/w) methanol and vortexed to get 10% (w/v) fecal homogenous solution. An aliquot of the fecal homogenate was stored at −20 °C overnight, and then centrifuged for 10 min at 10,000 ×*g* to collect the supernatant for GC (gas chromatography) analysis of SCFA as previously described by Power *et al.* (Power et al., 2016). 2-Ethylbutyric acid (Aldrich, #109959) as an internal standard was added into the supernatant. The supernatant was filtered through a 0.2 µm PVDF syringe filter and injected (1 µL) into the GC (Agilent 6890, Canada) which was equipped with a flame ionisation detector and a Nukol-capillary GC column (60 m × 0.25 mm × 0.25 µm, Sigma-24108 SUPELCO). Helium was used as the carrier gas; the initial oven temperature was 100 °C and was increased to 200 °C at a rate of 10 °C/min; injector and detector temperatures were maintained at 200 °C and 250 °C, respectively. The total run time was 20 min for each injection. The peaks of SCFAs and BCFAs (acetic, butyric, formic, isobutyric and isovaleric acids) were identified by comparing their retention times with volatile acid standard mix (Sigma, #46975-U).

2.9.2. Characterization of fecal metabolites by LC-MS/MS

Before conducting LC-MS/MS analysis, an aliquot of the mouse fecal extract was purified by StrataTM-X polymeric solid phase extraction (SPE) cartridges (200 mg, Phenomenex, Torrance, CA, USA) according to the manufacturer's instructions. The fecal metabolite fractions (from 12 replicated mouse samples) isolated by the ion exchange SPE column were subjected to mass spectrometry analysis. LC-MS/MS analysis was performed on a Thermo Scientific™ Q-Exactive™ Orbitrap mass spectrometer coupled to a Vanquish™ Flex Binary UPLC System (Waltham, MA, USA). Data were acquired using Thermo Scientific™ Xcalibur™ 4.2 software and Thermo Scientific™ Standard Integration Software (SII). The chromatographic separation was performed on a Kinetex XB-C18 100A HPLC column (100 × 4.6 mm, 2.6 µm, Phenomenex Inc., Torrance, CA, USA). The binary mobile phase consisted of solvent A (99.9% H_2O/ 0.1% formic acid) and solvent B (94.9% MeOH/ 5% ACN/ 0.1% formic acid). The following solvent gradient was used: 0–5 min, 0% to 12% B; 5–15 min, 12% to 23% B; 15–30 min, 23% to 50% B; 30 - 40 min, 50% to 80% B; 40–42 min, 80% to 100% B; 42–45 min, 100% B; 45–46 min, 100% to 0% B; 46–52 min, 0% B. The column compartment temperature was held at 40 °C, the flow rate was set at 0.700 mL/min, and the injection volume was 1 µL. Both positive and negative ionization modes were used; mass spectrometry data was collected using Full-MS/DDMS2 (TopN = 10) method, with NCE set at 30. Data was visualized and analysed using Thermo FreeStyle™ 1.5 software. Automated sample analysis was performed using Compound Discoverer 3.0 software. A modified template "Untargeted metabolomics workflow with statistics" was used to perform sample grouping, peak detection, identification of unknowns and differential analysis, and then the network of KEGG pathway was analyzed using MetaboAnalyst, and visualized using Cytoscape 3.8.0, an open-source software. Compound identification was based on elemental composition prediction and subsequent ChemSpider database search (FullMS) as well as spectral matching of MS/MS data with mzCloud library (MS^2).

2.10. Cecal microbiota analysis

2.10.1. 16S rRNA gene sequencing

Mouse cecal contents were collected in 2 mL screwcap microtubes and stored at −80 °C. Total DNA was extracted from the cecal samples using the QiaAmp DNA stool mini kit (Qiagen, #51504) according to the manufacturer's instructions. Briefly, cecal contents were mixed with buffer and InhibitEX (inhibitor cocktail) to collect supernatant after centrifugation at 10 000 ×*g* for 1 min, and then purified on QIAamp spin columns to remove contaminants. Sequencing libraries of the 16S rRNA gene were prepared according to the Illumina 16S Metagenomic Sequencing Library Preparation Guide Rev. B. Briefly, primers Bakt_341F (5′-CCTACGGGNGGCWGCAG-3′) and Bakt_805R (5′-GACTACHVGGGTATCTAATCC-3′) containing 5′ Illumina overhang adapter sequences (5′TCGTCGGCAGCGTCAGATGTGTATAAGAGACAG and 5′ TCTCGTGGGCTCGGAGATGTGTATAAGAGACAG, respectively) were used to amplify an ~537 bp fragment of the 16S rRNA V3-4 region. Each reaction containing 12.5 ng template DNA, 200 nM each primer and 1× KAPA HiFi HotStart ReadyMix (VWR, #CA89125-040) in a 25 µL volume was amplified using the following cycling conditions: 95 °C for 3 min, 25 cycles of 95 °C for 30 s, 55 °C for 30 s and 72 °C for 30 s, followed by 72 °C for 5 min. PCR products were purified with Ampure XP beads (Beckman Coulter, #A63881) and sequencing adapters containing 8-bp indices were added to the 3′ and 5′ ends by PCR using the Nextera XT Index kit (Illumina, #15055293) in a 50 µL reaction containing 5 µL PCR amplicon, 5 µL each indexing primer and 25 µL 2x KAPA HiFi HotStart ReadyMix using the following cycling conditions: 95 °C for 3 min, 8 cycles of 95 °C for 30 s, 55 °C for 30 s and 72 °C for 30 s, followed by 72 °C for 5 min. Following purification with AmpureXP beads, the amplicons were quantified using the Quant-iT PicoGreen double-stranded DNA assay (Invitrogen, #P7589), and pooled at equimolar ratios to a final concentration of 8 pM, combined with 10% equimolar PhiX DNA (Illumina, #FC1103001), and sequenced on a MiSeq instrument using the MiSeq 600-cycle v3 kit (Illumina, MS1023003).

2.10.2. Microbiota diversity analysis

Microbiota diversity analysis was performed with QIIME 2 v. 2019.7.0 (Bolyen et al., 2019). Briefly, 300 bp paired-end reads were processed with DADA2 to denoise reads, remove chimeric sequences and singletons, join paired-ends and dereplicate sequences to produce unique amplicon sequence variants (ASVs). Taxonomic classification of the resulting feature table was performed with Vsearch and the Greengenes 99% OTU sequences as reference. ASVs were discarded if they had fewer than 10 instances across all samples, were present in fewer than two samples, or were not assigned taxonomy at the phylum level. Multiple sequence alignment of ASV representative sequences was performed with MAFFT and a rooted phylogenetic tree constructed with FastTree. Core diversity analysis was performed using a sampling depth of 10,000 sequences to plot taxonomic relative abundances, calculate alpha-diversity metrics and generate dissimilarity matrices based on Bray-Curtis, Jaccard, and UniFrac distances, which were used for principal component (PCoA) analyses. Heatmaps and PCoA plots were generated with R and PhyloToast, respectively. Differential abundance testing was performed with ANCOM to identify taxa with significantly different relative abundances between treatment groups. Songbird was also used to calculate log-fold differentials for each ASV between treatment groups by multinomial regression,(Morton et al., 2019) and rankings were visualized with Qurro (Fedarko et al., 2020).

2.11. Statistical Analysis

Results were expressed as mean ± standard error of the mean (SEM) of at least triplicated measurements unless otherwise specified. Statistical analyses were carried out using GraphPad software (San Diego, CA, USA). The statistical significance of the data was determined using two-way or one-way ANOVA followed by Tukey's multiple-comparison test with a $p < 0.05$ taken as value of significance. One-way ANOVA followed by Tukey's post hoc test and data visualization of body weight change data were conducted using "Paired Comparison Plot" app of the OriginPro 2021 (OriginLab Corporation, Northampton, MA, USA).

3. Results and discussion

3.1. Effect of PPE on metabolic homeostasis and risk of developing metabolic disorders

Impaired balance of the immune-metabolic axis leads to dysregulation of energy storage and insulin sensitivity that further contributes to the pathogenesis of obesity and type 2 diabetes (Kotas and Medzhitov, 2015). The anthocyanin-rich extract used in the present study was the same as in our previous studies (Hua Zhang et al., 2016), i.e., it contains 26% total anthocyanins or 54% by chromatographic peaks. In vitro digestion and cell models showed that the bioaccessibility and bioavailability of anthocyanins of purple potato were 71.8% and 37%, respectively, and the predominant anthocyanin, petunidin-3-O-p-coumaroylrutinoside-5-O-glucoside was found to be transported in its intrinsic form (H. Zhang et al., 2017). In the present study, supplementation of both low- and high-dose PPE exhibited significant inhibition on the overall body weight gain caused by HFD or HFD+LPS administration in mice, especially after week 12. In particular, mice treated with the high dose PPE showed consistently stronger reduction of body weight gain than the low-dose treatment albeit the difference was not statistically significant (Figure 2a). Results from the GTT (AUC, within 2 h) also showed that both low- and high-dose PPE treatments significantly down-regulated the blood glucose AUC elevated by HFD or HFD+LPS (Figure 2b). Plasma insulin level was significantly elevated in mice of the HF or HF/LPS group as compared to that in NC. While the difference in plasma insulin levels of the LPP or HPP in mice was not statistically significant from that in the HF or HF/LPS group, bother treatment groups, especially the HF group, showed a moderately decreased level compared to the two control groups (Figure 2c). These results clearly demonstrate that the anthocyanin-rich extract from purple potatoes acts on glucose metabolism, in the case of obese mice induced by HFD or HFD/LPS. In addition to glucose metabolism, the effect of PPE supplementation on lipid metabolism was also assessed. In general, HDF or HDF+LPS increased the plasma triglyceride, total cholesterol and LDL concentrations in mice to significantly higher levels than normal diet. However, the elevated plasma triglyceride and total cholesterol concentrations were greatly lowered by PPE at both doses (Figure 2d and e). Mice in the HPP group showed significant reduction in total cholesterol concentration from those in the HF/LPS group (Figure 2e). The effect of PPE on LDL was more significant, especially at higher dose which significantly reduced the plasma LDL compared to those in the HF and HF/LPS

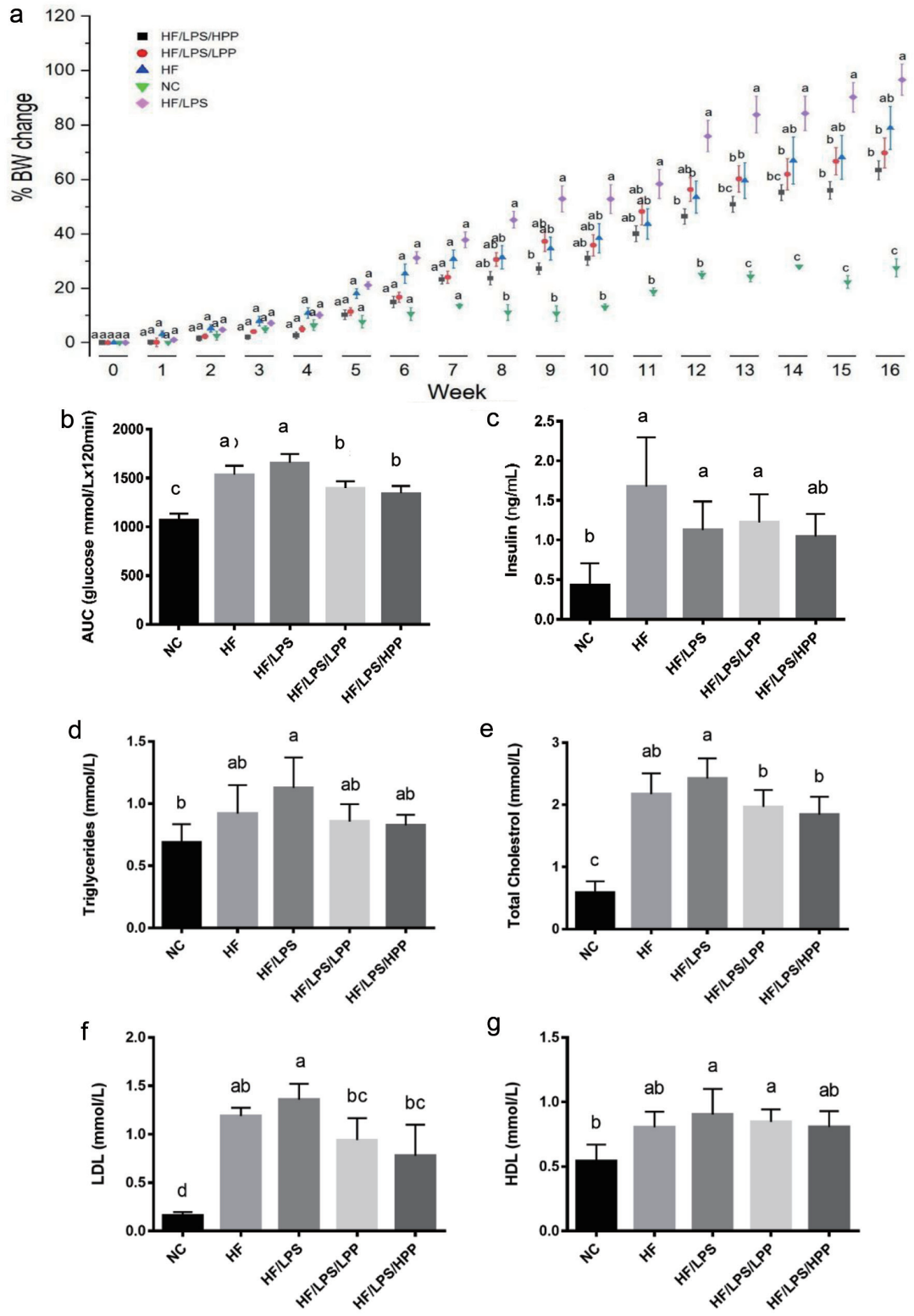

Figure 2. Effects of purple potato extract (PPE) on body weight gain, plasma glucose and insulin levels and lipid profile. a), percent average body weight gain (n = 12); b), AUC of glucose tolerance test; c), plasma insulin concentration; d), plasma lipid profile, triglyceride; e), cholesterol; f), HDL cholesterol and g), LDL cholesterol. The negative control (NC) group represents the mice that have a normal diet, while the HF/LPS and HF represent the mice administered with HFD with or without LPS. The mice pre-treated with PPE at low and high doses are designated LPP and HPP, respectively. Results are represented as means ± SEM, n = 6. Values without a common letter are significantly different at $p < 0.05$.

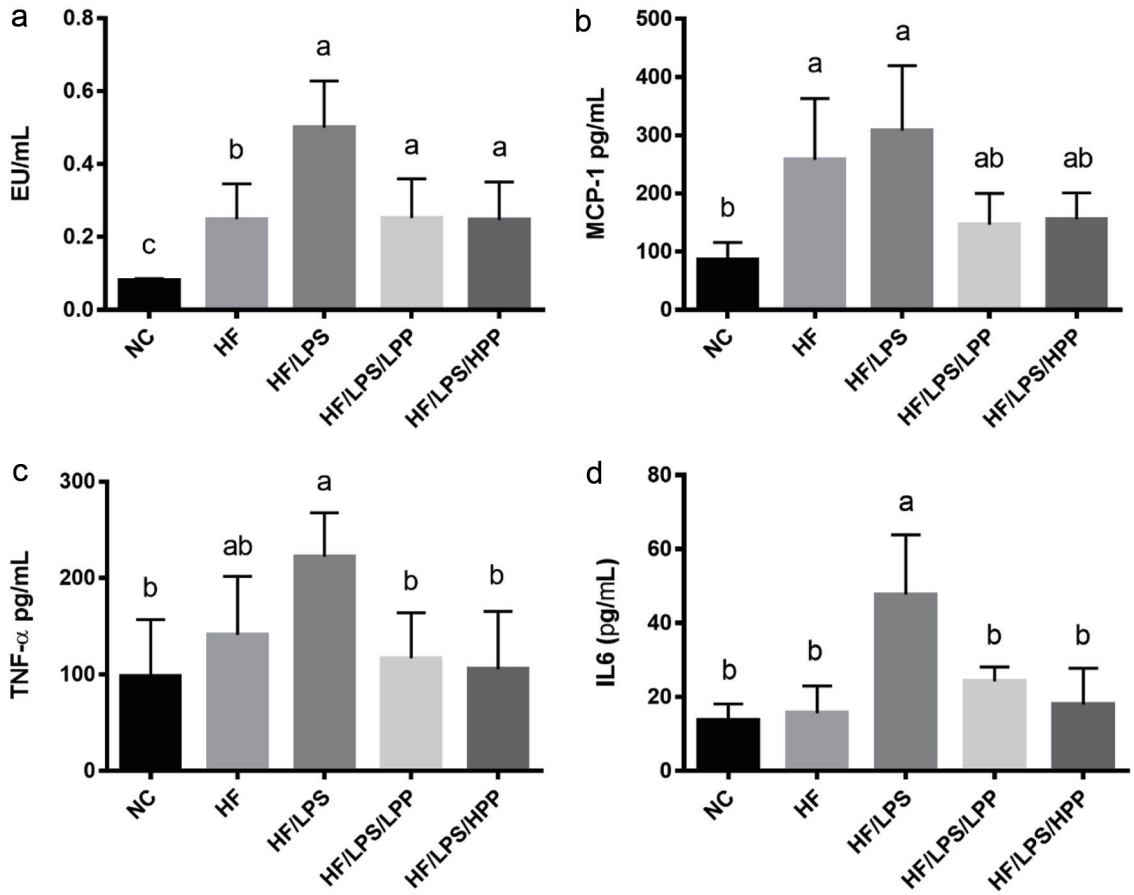

Figure 3. Effects of purple potato extract (PPE) on plasma concentrations of endotoxin and pro-inflammatory cytokines. a), endotoxin; b), MCP-1; c), TNF-α; d), IL-6. The negative control (NC) group represents the mice that have a normal diet, while the HF/LPS and HF represent the mice administered with HFD with or without LPS. The mice pre-treated with PPE at low and high doses are designated LPP and HPP, respectively. Results are represented as means ± SEM, n = 6. Values without a common letter are significantly different at $p < 0.05$.

controls (Figure 2f). Plasma HDL was increased in all groups of mice except the NC, but no significant effect was shown by PPE (Figure 2g). This indicates that PPE supplementation affects the total plasma cholesterols mainly by lowering LDL (Figure 2d-g). Collectively, our results indicate that PPE supplementation can improve metabolic profile toward energy homeostasis by lowering plasma glucose, triglycerides, total cholesterol and LDL concentrations. Maintaining metabolic homeostasis can ultimately lead to reduced risk of developing metabolic disorders.

3.2. Effect of PPE on endotoxemia and its mediated dysfunctions in WAT

3.2.1. Inhibitory effect of PPE on HFD and LPS induced endotoxemia

The existence of endotoxin such as LPS in the circulation system elicits chronic systemic inflammation that enhances the distribution of activated macrophage (M1) into WAT (Cani, 2018). The inflamed WAT subsequently secretes free fatty acids (FFA) to augment the local inflammatory responses. In this study, a significant increase in plasma endotoxin level was observed in the HF mice compared to the NC mice. The increase of the plasma endotoxin in HF+LPS mice was even more significant, higher than in mice of all groups (Figure 3a). This suggests that administration of LPS can further elevate the endotoxemia in HFD fed mice. Pre-treatment with both low- and high-dose PPE significantly suppressed the plasma concentration of endotoxin compared to the HF/LPS group (Figure 3a). Further study showed that plasma pro-inflammatory cytokines, including MCP-1, IL-6 and TNF-α, were all significantly elevated by HFD and HFD+LPS; however, all pro-inflammatory markers induced by these unhealthy dietary factors were effectively alleviated by PPE supplementation at both doses, and in the case of plasma IL-6 and TNF-α, the effect was statistically significant compared with those in the HF/LPS group (Figure 3b-d). These results indicate that PPE supplementation can significantly inhibit the development of endotoxemia and subsequent systemic inflammation induced by HFD and LPS.

3.2.2. Effect of PPE on endotoxemia-mediated dysfunctions in WAT

Increased incidence of endotoxemia in the mice treated with HFD and LPS strongly supports the findings in previous studies in which endotoxemia was shown to impair adipose metabolic function (Mehta et al., 2010). As stated above, intake of HFD or HFD+LPS

resulted in increased level of endotoxin in the circulation system that provoked a cytokine storm in significantly augmented secretion of systemic inflammatory responses (Figure 3b-d). Research have shown that a prolonged intake of HFD promotes adipogenesis and enlarges the size of subcutaneous abdominal adipocytes, leading to progressive adipocyte hypertrophy and insulin resistance. In addition to upregulated inflammatory tone, the progression of adipocyte hypertrophy also increases the release of FFA and TNF-α in WAT to recruit active M1, leading to the development of on-site inflammation which in turn impairs metabolic homeostasis in WAT (Suganami et al., 2005). The subcutaneous abdominal adipocytes were significantly enlarged and were accompanied by apparent macrophage infiltration as characterized in crown-like structures in WAT of mice fed HFD or HFD+LPS compared to those fed normal diet (Figure 4a). This significant increase of macrophage infiltration is a clear indication of inflammation in WAT caused by unhealthy diet. However, PPE supplementation not only significantly suppressed the progression of adipocyte hypertrophy in the subcutaneous WAT (Figure 4a), but both low- and high-dose PPE supplementation significantly inhibited macrophage infiltration induced by HFD or HFD+LPS (Figure 4b). The onsite inflammatory events in WAT is known to eventually cause metabolic dysfunctions such as in adipogenesis and insulin sensing. In this study, HFD or HFD+LPS, particularly the latter caused a significant decrease in adipose adiponectin level (Figure 4c). However, supplementation of PPE at both doses showed a strong ability in restoring the adiponectin secretion in WAT to the same level as that in mice fed normal diet (Figure 4c). Adiponectin is a hormone secreted in adipose tissue that modulates glucose regulation. Meanwhile, expression of PPAR-γ, a nuclear receptor protein that regulates fatty acid storage and glucose metabolism, was found to be significantly downregulated in mice fed HFD+LPS, but supplementation of PPE at either low- or high- doses effectively and significantly reversed the level of PPAR-γ to the same as in NC mice (Figure 4d). Similarly, IRS-1 expression in WAT was also significantly suppressed as a result of HFD or HFD/LPS, and supplementation with PPE at both doses effectively restored the IRS-1 expression, although only that in the WAT of HPP mice was significantly higher compared to the HF/LPS mice. The restoration of IRS-1 expression was also nearly complete compared to that in the NC mice (Figure 4e). Low IRS-1 expression can lead to the development of glucose dysregulation and insulin resistance. Results of the present study showed that PPE supplementation not only significantly reduced adipocyte hypertrophy and macrophage infiltration induced by HFD and HFD+LPS, but it also positively modulated the expression of adiponectin, PPAR-γ and IRS-1 proteins. Dietary PPE enriched in anthocyanins is therefore a potential approach to successful restoration of energy metabolic homeostasis. PPE can inhibit HFD and LPS-induced inflammatory responses and related impairment of metabolic dysfunctions in the adipocytes. Activation of PPAR-γ and IRS-1 causes insulin sensitization and enhances glucose metabolism; however, the mechanisms underlying all observed data are still unknown and need to be further investigated.

3.3. Effect of PPE on gut barrier function

HFD, particularly diet high in saturated fat, and LPS can elicit inflammatory responses in the gut epithelium and lead to the alterations of intestinal tight junction (TJ) protein expressions. Diet can also change composition of gut microbiome and cause epigenomic modifications at the site of intestinal epithelium, contributing to a broad range of immune responses and inflammatory diseases (Peterson and Artis, 2014). For this reason, we examined the immunoregulatory properties of PPE and the effects on the gut barrier to better understand the preventive mechanisms of these food bioactives in alleviating multiple inflammatory and metabolic diseases. The existence of D-mannitol in the blood is an indication of a leaky gut, thus in this study, we measured blood D-mannitol concentration to assess the intestinal permeability of the gut epithelium. Compared to the NC mice, those in the HF+LPS group had significantly higher concentration of D-mannitol, suggesting unhealthy diet can indeed cause damage to the gut epithelium (Figure 5a). PPE supplementation effectively lessened the permeation of D-mannitol into the blood in HFD/LPS-induced mice, and the effect was most significant in HPP mice. The result that high-dose PPE can effectively restore the HFD/LPS-induced D-mannitol to the same level as that in NC mice suggests a strong protective ability by PPE against leaky gut (Figure 5a). The TJ protein expressions in the jejunum and colon were also evaluated to determine the effect of PPE supplementation on gut barrier integrity. In the jejunum, while the expressions of TJ proteins, zonula occluden (ZO)-1, junctional adhesion molecule (JAM)-A and claudin3 (Cld3) were drastically lowered in HFD or HFD+LPS mice, those in mice pre-treated with PPE showed significant improvement, particularly at the high-dose which completely restored the ZO-1 and JAMA expressions to the levels in mice fed normal diet. In terms of Cld3, although no statistically significance was found, PPE supplementation at both doses restored partially the HFD- or HFD/LPS-induced decrease of this protein (Figure 5b). The expressions of a series of more TJ proteins of the colon were also examined, and were found to be mostly suppressed by HFD or HFD+LPS, but in general, the lowered expressions were significantly upregulated by PPE supplementation, especially at the high-dose (Figure 5c). Deficiency of TJ proteins increases para-cellular gap and permeability, allowing luminal stimuli such as antigens, commensal microbiome and toxins to enter into the intestinal submucosal layer to stimulate the innate immune response, leading to ultimate development of gut inflammation. Our results on the effects of PPE on major pro-inflammatory cytokines i.e. MCP-1, TNF-α, IL-6, IL-1β, IL-17A and the anti-inflammatory cytokine IL-10 corroborated the above conclusion (Figure 5c). The high pro-inflammatory cytokines (i.e. IL-6, IL-1β, IL-17A) induced by HFD/LPS were significantly downregulated, and IL-10 upregulated by PPE at high dose. Our results indicate that along with the protective effect on the gut barrier integrity, high dose PPE supplementation can significantly attenuate the colonic inflammation by reducing pro-inflammatory cytokine expression and restoring anti-inflammatory cytokine IL-10 expression (Figure 5c). This also implies that dietary PPE can potentially protect the intestinal epithelium and improve gut barrier functions against inflammatory stimuli.

3.4. Mechanism of the protective effect of PPE on gut barrier function

3.4.1. The modulatory effect of PPE on gut sensing activity

The primary defensive line of the human gut consists of the intestinal epithelial cells (IEC)-derived mucins, anti-microbial proteins and receptors. The receptors distributed along the IECs contribute to recognition of luminal symbiotic microbiota to regulate the mucosal immune responses thereby promoting IEC health and function (Peterson and Artis, 2014). The various pattern recognition receptors (PRRs), such as the toll-like receptor (TLR) and nucleotide

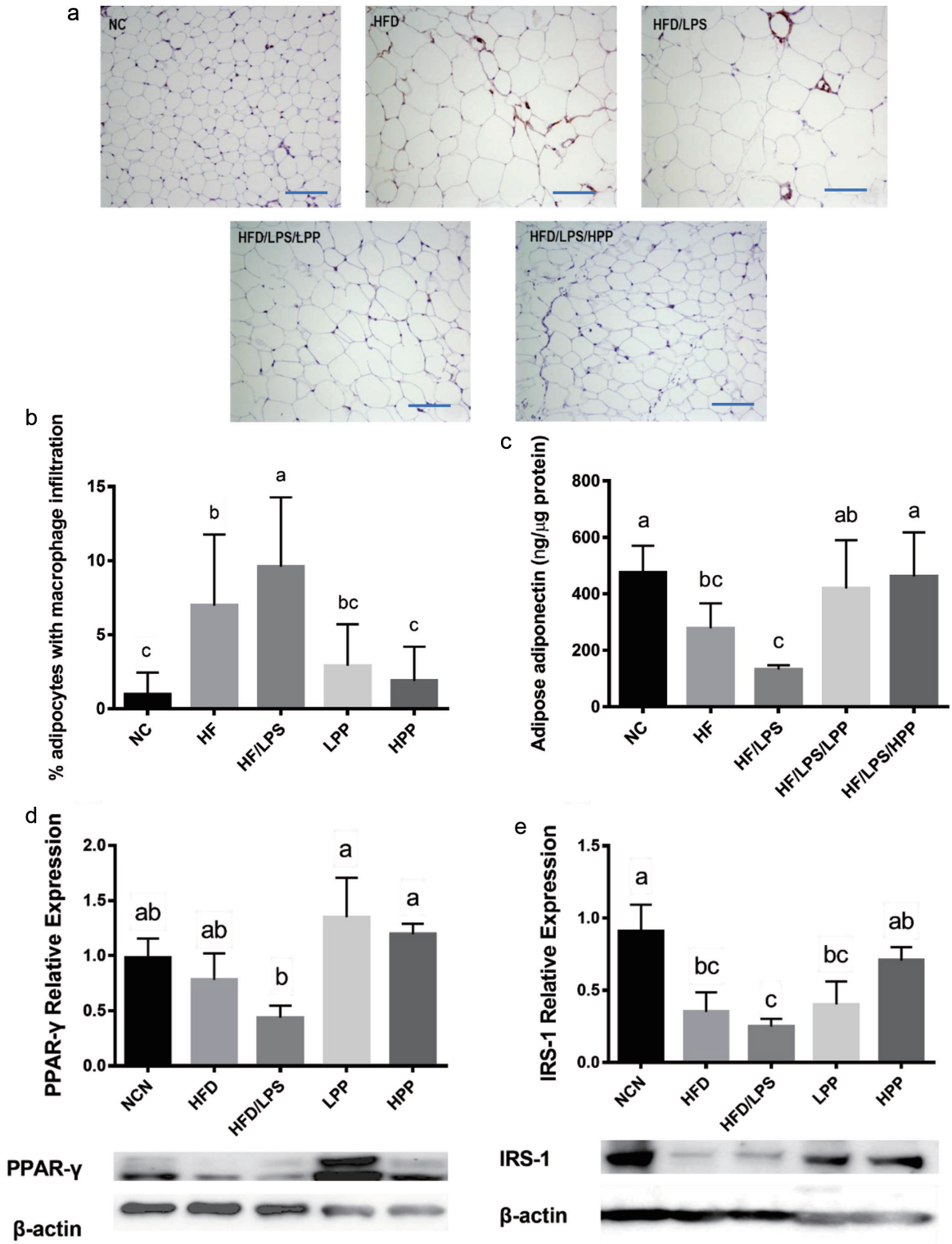

Figure 4. Effects of purple potato extract (PPE) on macrophage infiltration, adiponectin and protein expression in white adipose tissues (WAT). a), immuno-histochemical images of WAT. Scale bar represents 20 μm; b), percentage of adipocytes with macrophage infiltration (crown-like structure) in WAT; c), adiponectin in WAT; d), PPAR-γ and E) IRS-1 protein expression in WAT. β-actin was used as reference protein. The negative control (NC) group represents the mice that have a normal diet, while the HF/LPS and HF represent the mice administered with HFD with or without LPS. The mice pre-treated with PPE at low and high doses are designated LPP and HPP, respectively. Results are represented as mean ± SEM, n = 12 for panels A-C; n = 6 for panels D and E. Values without a common letter are significantly different at $p < 0.05$.

a

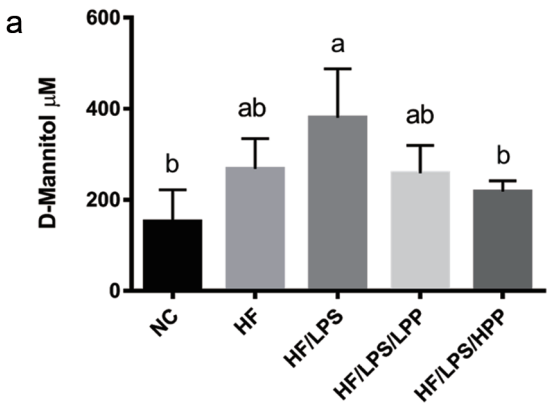

b

Jejunum	NC	HFD	HFD/LPS	LPP	HPP
ZO-1	136.0±28.68a	1.32±0.42b	0.73±0.28b	48.21±13.11a	155.54±31.39a
JAMA	194.0±14.49a	2.15±0.86b	1.36±0.64b	164.23±22.17a	195.80±44.19a
Claudin3	4.15±0.70a	1.26±0.35b	1.14±0.28b	1.96±0.30b	2.22±0.31b

c

Colon	NC	HFD	HFD/LPS	LPP	HPP
ZO-1	7.69 ± 1.38^{a}	1.30 ± 0.41^{b}	2.5 ± 0.81^{b}	5.61 ± 1.05^{a}	7.51 ± 1.64^{a}
JAMA	1.57 ± 0.15^{a}	0.91 ± 0.09^{b}	0.97 ± 0.05^{b}	1.19 ± 0.2^{b}	1.69 ± 0.11^{a}
Claudin1	3.56 ± 0.49^{a}	0.98 ± 0.32^{b}	1.31 ± 0.06^{b}	3.05 ± 0.71^{a}	3.38 ± 0.64^{a}
Claudin3	3.62 ± 0.44^{a}	1.56 ± 0.37^{a}	1.22 ± 0.24^{b}	2.71 ± 0.42^{a}	2.78 ± 0.65^{a}
Occludin	6.97 ± 1.05^{a}	1.80 ± 0.5^{b}	1.38 ± 0.33^{b}	4.27 ± 1.0^{b}	6.11 ± 0.82^{a}
Muc2	1.13 ± 0.2^{a}	0.93 ± 0.34^{b}	0.85 ± 0.21^{b}	0.74 ± 0.17^{b}	1.52 ± 0.32^{a}
MCP-1	1.37 ± 0.38^{a}	1.22 ± 0.12^{a}	3.04 ± 0.66^{b}	0.42 ± 0.19^{a}	0.5 ± 0.16^{a}
TNF-α	1.06 ± 0.13^{a}	2.19 ± 0.38^{a}	3.72 ± 0.93^{b}	1.59 ± 0.31^{a}	0.87 ± 0.37^{a}
IL-6	1.21 ± 0.33^{a}	6.21 ± 1.9^{b}	7.38 ± 1.8^{b}	3.36 ± 2.35^{a}	1.62 ± 0.64^{a}
IL-1β	1.09 ± 0.22^{a}	41.18 ± 12.54^{b}	35.7 ± 9.64^{b}	8.30 ± 1.82^{a}	8.26 ± 1.83^{a}
IL-17A	1.25 ± 0.31^{a}	94.25 ± 19.90^{b}	111.17 ± 28.05^{b}	31.54 ± 25.52^{a}	15.43 ± 4.16^{a}
IL-10	1.6 ± 0.28^{a}	0.41 ± 0.09^{b}	0.146 ± 0.08^{b}	0.27 ± 0.24^{b}	1.09 ± 0.25^{a}

Figure 5. Modulatory effect of purple potato extract (PPE) on intestinal integrity related markers. a), on plasma D-mannitol level; b), on tight junction proteins in tissues of jejunum; c), on tight junction proteins and pro- and anti-inflammatory cytokines and in tissues of colon. The negative control (NC) group represents the mice that have a normal diet, while the HF/LPS and HF represent the mice administered with HFD with or without LPS. The mice pre-treated with PPE at low and high doses are designated LPP and HPP, respectively. Results are represented as mean ± SEM, n = 6. Values without a common letter are significantly different at $p < 0.05$.

oligomerization domain (NOD)-like receptor (NLR), play a key role in sensing pathogens or alteration of symbiotic microbiota, and in initiating the innate responses (Chu and Mazmanian, 2013). The anti-microbial antibody IgA and pathogen recognition receptors TLR4, NOD2, Reg3β and Reg3γ in the colon tissues of mice fed HFD were significantly suppressed compared to those in mice fed normal diet. This suggests that HDF is implicated in the deficiency of gut mucosal immunity possibly by weakening the gut sensing activity. Other receptors were less sensitive to HFD (Figure S1). Our results also showed that due to its specific ability in recognizing LPS, TLR4 expression was significantly upregulated by the addition of LPS to HFD (Figure S1). The upregulated TLR4

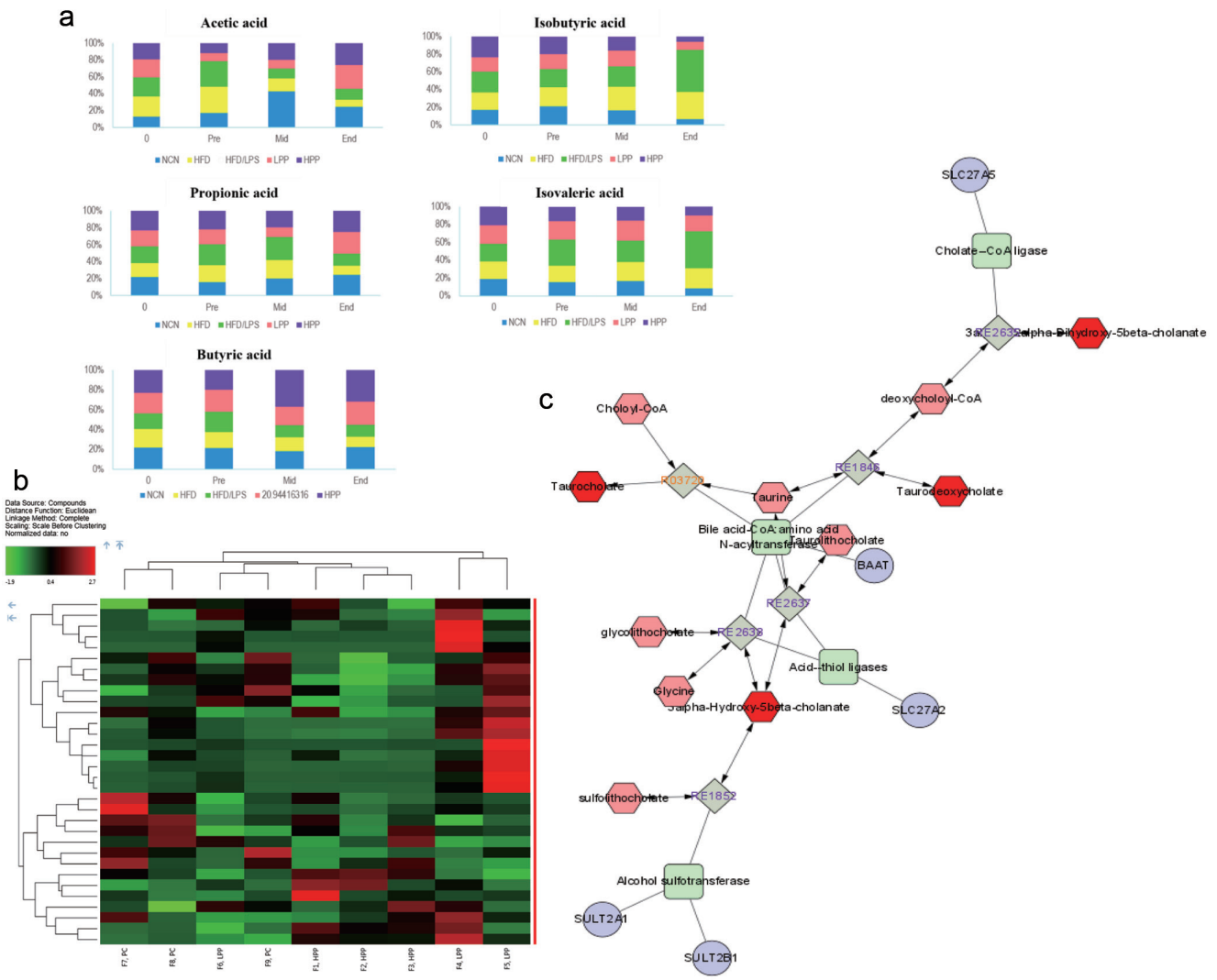

Figure 6. Supplementation of purple potato extract (PPE) regulates intestinal metabolism. a), on fecal microbial-derived SCFAs and BCFAs; b), a heat-map of fecal metabolites; and c), metabolic pathway networks regulated by HPP treatment. Fresh fecal samples were collected from mice in the following treatment groups. The negative control (NC) group represents the mice that have a normal diet, while the HF/LPS and HF represent the mice administered with HFD with or without LPS. The mice pre-treated with PPE at low and high doses are designated LPP and HPP, respectively. Results are represented as mean ± SEM, n = 6. Values without a common letter are significantly different at $p < 0.05$.

expression can lead to enhanced activation of the pro-inflammatory NF-κB pathway and apoptosis in the IECs (Villena and Kitazawa, 2014). However, our results showed that the upregulated expression of TLR4 was significantly reduced by both low- and high-dose of PPE, indicating an anti-inflammatory action of PPE. In addition, PPE supplementation was also shown to attenuate the upregulated expression of PRRs (i.e. TLR4, NOD2, Reg3β and Reg3γ) and IgA induced by LPS+HFD, and the attenuation was significant at high dose (Figure S1). Collectively, our study suggests that intake of PPE can potentially improve intestinal defence against stimuli and restore gut immune homeostasis.

3.4.2. Effect of PPE on microbial-derived metabolite profile in feces

Fecal samples were collected at the beginning (0 day), before HFD and LPS stimulation, middle point and endpoint of the trial, and the microbiota associated SCFAs (i.e. acetic, propionic, and butyric acids) and branched chain fatty acids (BCFAs) (i.e. isobutyric and isovaleric acids) were analyzed by GC. Our results showed that although individual SCFAs appeared to be similar among mice of different experimental groups, there were gradual changes in SCFC and BCFA profiles (Figure 6a). Distributions of SCFAs or BCFAs were modified by HFD or HFD+LPS and by PPE supplementation. Conspicuous reduction of SCFAs and increase of BCFAs were found in fecal samples of mice fed HFD or HFD+LPS. However, in mice fed PPE, especially in those fed a high dose and collected at the endpoint, reduction in SCFAs was reverted to even higher concentrations than that in feces of mice before introducing to HFD or HFD+LPS. The opposite was true for the BCFAs, i.e. PPE treatment at high dose greatly reduced the BCFAs at the endpoint compared to those at the beginning of the experiment (Figure 6a). There were some unexplainable variations such as the acetic

acid concentration in feces of NC mice; however, the general trend of our data showed that PPE supplementation indeed favored the production of SCFAs, especially butyric acid. Increased SCFAs production contributes to regulation of gut-associated lymphocyte sensing activity by binding with metabolite-sensing G protein-coupled receptors GPR41 and GPR43, which result in an intestinal immune homeostasis (Gibson et al., 2004). SCFAs, especially butyric acid is known to inhibit NF-κB-induced pro-inflammatory mediators e.g. TNF-α and IL-6 expression and increases anti-inflammatory mediators (e.g., IL-10). Butyric acid is also the main source of energy for colonocytes (Parada Venegas et al., 2019). On the other hand, BCFAs such as the isobutyric and isovaleric acids found in fecal samples of the present study reflect proteolytic metabolism, and are generally considered to impact negatively on gut health although the exact role of BCFAs are not clear (Millet et al., 2010; Rios-Covian et al., 2020). Our data also suggests that anthocyanins/polyphenols may have altered the microbiota composition in favour of SCFA-producing bacteria. Polyphenols and their metabolites are known to contribute to the maintenance of gut health by exerting prebiotic-like effects (Cardona et al., 2013). Dietary anthocyanin-rich polyphenols have also been shown to alter the gut microbiota composition by phenolic metabolites (Mosele et al., 2015). The increase in fecal SCFAs and decrease in fecal BCFAs in PPE fed mice are therefore a strong indication that anthocyanin-rich polyphenols of purple potato may modulate gut microbiota and consequently the profile of microbial fermentation products in favour of enhanced immune response and gut health.

In addition to the SCFAs, metabolomics studies were also carried out for pooled fecal samples using LC-MS/MS, to obtain metabolomic profile linked to the colonic microenvironment. The colonic metabolites are crucial attributes of intestinal homeostasis that enables the establishment of a stable environment permissive to colonization by commensal bacteria, leading to an integrated regulation of immune-metabolic axis. The metabolomics study was only performed in selected PPE supplemented as well as HFD/LPS fed mice and the results are shown in Figure 6b and c and Figure S2. The LC-MS/MS metabolomic heat map illustrates distribution of metabolites of fecal samples of mice in these experimental groups (Figure 6b). A close analysis of the metabolomic profiles ascertained that intake of PPE was involved in regulating the intestinal bile acid metabolic pathway; colored bile acid metabolites identified in Figure S2 are the ones involved in the regulatory functions of bile secretion. Enteric dysfunction is strongly associated with altered bile acid metabolism. Compared with the HFD/LPS group, mice fed high dose PPE upregulated the secretion of bile acid in the form of glycine conjugate or glycocholic acid (GCA) and a secondary bile acid 1-β-hydroxycholic acidor ursodeoxycholic acid (UDCA), while downregulated cholestenoic acid 3β,7α-dihydroxy-5-cholestenoate (Figure S2). The increased secretion of 3β,7α-dihydroxy-5-cholestenoate is associated with hepatic bile acid synthesis (Honda et al., 2004). It is likely that the inhibition of fecal cholestenoic acid by the anthocyanin-rich extract of purple potato may result in better control of hepatic fat metabolism, thus can lower the risk of developing fatty liver disease. Furthermore, UDCA is a metabolic byproduct of gut microbiome and has been shown to have anti-inflammatory effect on IECs (Ward et al., 2017). There is a strong correlation identified between UDCA and the bacterial genus *Holdemanella* and *Veillonella* (Martin et al., 2018). In terms of the low dose PPE treatment, despite the higher variation it was also shown to regulate the bile acid synthesis by upregulating taurochocholic acid (TCA) and taurochenodeoxycholic acid (TCDCA) while downregulating deoxycholic acid (Figure S2). Subsequently, MetaboAnalyst was applied to perform a comprehensive analysis of metabolic networks (Figure 6c). Results indicated that metabolic pathways of the bile acid biosynthesis, tyrosine metabolism, tryptophan metabolism, and purine metabolism were regulated by PPE against low-grade inflammation associated with obesity (Figure 6c). It has been found that TCA abundance is positively correlated with the bacterial genus *Akkermansia* and *Parasutterella,* and TCDCA is positively correlated with that of the genus *Eubacterium* (Martin et al., 2018). The excess fecal bile acids produced by *Clostridia* bacteria is considered to play a role in developing irritable bowel syndrome (IBS) (Zhao et al., 2019). However, linkage between the microbial metabolites and gut microbiota under a particular disease condition such as that induced by HFD/LPS in the present study is far more complex than conventional beliefs (Liu et al., 2019). The fecal bile acids are the intestinal nuclear farnesoid X receptor (FXR) and G protein-coupled membrane receptor 5 (TGR)-5 antagonists. By interacting with FXR, colonic bile acids can trigger the signaling transductions in IECs that are involved in regulating numerous metabolic pathways of energy expenditure, fat metabolism and glycemic control of the host. The colonic bile acids are also directly or indirectly implicated in modulation of gut microbial composition through activation of innate immune responses (Wahlström et al., 2016). Nevertheless, our findings that alterations in fecal bile acid profile caused by PPE can be considered beneficial outcomes in that they contribute to an enhanced intestinal metabolic and immune function.

3.5. Effect of PPE on colonic microbial community structure

To assess the impact of PPE at either low or high dose on dominant gut bacterial communities, 16S rRNA gene libraries were prepared from the total cecal DNA and the diversity of the enteric microbiota were subsequently analyzed. Following denoising, chimera removal, quality filtering, and assembly of paired-ends, the resulting ASVs were assigned taxonomy and used to assess the microbial community structure. At the family level, the cecal microbiota of all treatment groups was dominated by four phyla consisting of approximately ten family members, including *Bacteroidetes* (S24-7, *Bacteriodaceae, Rikenellaceae, Odoribacteraceae, Porphyromonadaceae*), *Firmicutes* (*Ruminococcaceae and Lachnospiraceae*), *Proteobacteria* (*Desulfovibrionaceae*) and *Verrucomicrobia* (*Verrucomicrobiaceae*) (Figure 7a). The alpha-diversity of the HPP-fed group was significantly higher (corrected p-value < 0.05, Kruskal Wallis) than other groups, except for the HF/LPS group, in measures of both species richness (Chao1) and richness/evenness (Shannon) (Figure 7b). Similarly, beta-diversity also differed significantly between all groups (corrected p-value < 0.05; permanova) using both qualitative (Jaccard) and quantitative (Bray-Curtis) metrics, and weak clustering of groups could be observed in principal coordinate analysis (PCoA) plots of the respective distance matrices (Figure 7c and d). Differential abundance testing was performed with both ANCOM and Songbird to identify specific taxa that contribute to these group differences. ANCOM analysis identified *Ruminococcus gnavus*, and three unknown species of the genera *Prevotella*, *Bilophila* and *Bacteroides* as having significantly different relative abundances among the five treatment groups, in which differences were principally observed between groups receiving a HF diet compared with the NC group (Figure 7e). Songbird was used to calculate log-ratios differentials between treatment groups compared to the HF/LPS group using a multinomial regression model. Ranking of ASV differentials calculated from the HPP identified taxa positively and negatively associated with mice fed a high-dose of PPE (Figure 7f). The ASVs positively associated with the HPP group (Table S2)

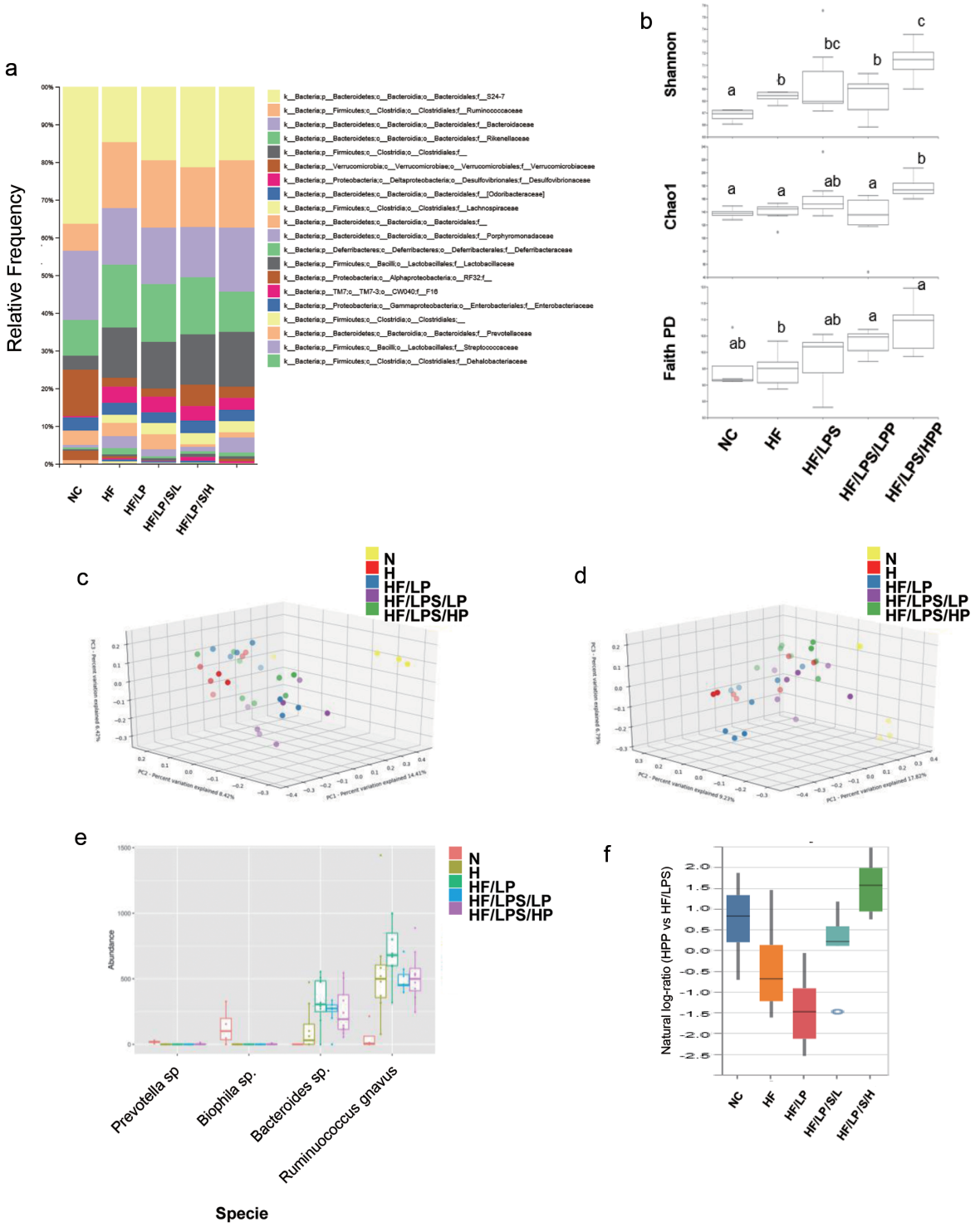

Figure 7. The impact of purple potato extract (PPE) on beta-diversity and community structure of fecal microbiota. a), relative abundances of microbial taxonomic groups at the family level; b) alpha-diversity of microbial communities from each treatment group based on Shannon, Chao1 and Faith Phylogenetic Diversity metrics. Statistically significant differences between groups (Kruskal-Wallis, $p < 0.05$) are indicated by different letters; c) and d), samples were clustered by principal coordinate analysis (PCoA) of Jaccard (c) or Unweighted UniFrac (d) distance matrices. The first three principal coordinates (PC1, PC2, PC3) are plotted for each mouse; e), absolute abundances of bacterial species identified as differentially abundant between treatment groups by ANCOM analysis; f), Differential abundance results of ASVs associated with the HPP group, using the HF/LPS group as reference, identified by Songbird analysis and visualized with Qurro. The top 10% of positively- and negatively-associated ASVs were used as numerator and denominator, respectively, for plotting natural log ratios. The associated ASV are given in Table S2.

included several species of the genera *Oscillospira* and *Parabacteroides*, as well as *Bacteroides acidifaciens* and *Akkermansia muciniphila,* while the negatively-associated ASVs were dominated by members of the Rikenellaceae family. Results from the metabolomics profiling (Figure 6) and gut microbiome analysis (Figure 7) collectively suggest a clear relationship between the features of the gut microbiota and fecal metabolites, pointing to a new direction for future studies to better understand the impact of PPE or its major component (anthocyanins) on the host-gut microbiota interplay and its role in the prevention of developing metabolic disorders.

In summary, our results showed that early introduction and sustained supplementation with PPE, especially at high dose (100 mg/kg BW), 3 times a week by oral gavage contributed to the maintenance of systemic metabolic homeostasis by significantly reducing the body weight gains and lowering blood glucose level, and to some degree plasma insulin concentration induced by HFD and/or HFD/LPS (Figure 2a-c). PPE also significantly improved the plasma lipid profiles by significantly lowering the plasma triglyserides and total cholesterols. The latter effect was mainly from the significant reduction in LDL (Figure 2d-g). Further studies showed that the anthocyanin-rich PPE prevented HFD and/or HFD/LPS-induced endotoxemia as shown in significantly reduced plasma endotoxin concentrations and associated pro-inflammatory cytokines MCP-1, IL-6 and TNF-α, suggesting a strong inhibitory effect on systemic inflammation (Figure 3). The significant anti-inflammatory effect of PPE was also evident in alleviating adipocyte hypertrophy and macrophage infiltration, and in complete restoration of adiponectin in the WAT, and nuclear receptor proteins PPAR-γ and IRS-1 that regulate fatty acid storage and glucose metabolism (Figure 4). These findings clearly demonstrated the role of dietary anthocyanin-rich PPE in modulating energy storage and metabolism and systemic inflammatory status, and the potential in preventing unhealthy diet e.g. HFD/LPS-induced metabolic syndromes and diseases such as obesity and type 2 diabetes. PPE supplementation significantly improved gut barrier function by preventing gut leaking as shown in significantly inhibited D-mannitol concentration in the blood (Figure 5a), and by attenuating damage caused by HFD/LPS in intestinal tight junction as seen in restored TJ proteins ZO-1 and JAM-A in the jejunum and additional proteins and pro-inflammatory cytokines in colon tissues (Figure 5b). PPE supplementation especially at high dose significantly upregulated the expression of TJ proteins ZO-1, JAM-A, Cld3, claudin and muc2, downregulated the pro-inflammatory cytokines MCP-1, TNF-α, IL-6, IL-1β, IL-17A and upregulated the anti-inflammatory cytokine IL-10 induced by HFD/LPS in the colon (Figure 5b). Meanwhile, at the intestinal epithelial layer, PPE supplementation apparently also showed anti-inflammatory effect by significantly suppressing the expression of HFD/LPS-induced upregulation of IgA and several PRRs including TLR4, NOD2, Reg3β and Reg3γ in the colon tissues. Downregulation of receptors such as TLR4 is known to inhibit activation of the NF-κB pathway and apoptosis in the IECs (Figure S1). These data corroborated with other results of the present study and collectively they indicate that PPE supplementation can potentially improve intestinal defence against stimuli and restore gut immune homeostasis. Increased SCFAs and reduced BCFAs detected in the fecal samples of mice fed PPE further suggest that anthocyanins/polyphenols or their metabolites may have altered the microbiota composition in favour of SCFA-producing bacteria, thus having prebiotic-like effects (Figure 6a). Metabolomics profiling indicates that the intake of PPE was involved in regulating the intestinal bile acid metabolic pathway, an indication of altered bile acid metabolism that may potentially lead to enhanced intestinal metabolic and immune functions (Figure 6c). 16S rRNA analysis of the total fecal DNA showed that high dose PPE increased Firmicutes population compared to the HFD/LPS control, and promoted the growth of *P. distasonis,* a novel probiotic that regulates metabolic bile acids to alleviate metabolic dysfunctions in the gut (Figure 7). All these results suggest that pretreatment of PPE can reduce the colonic pro-inflammatory cytokine production, maintain TJ (e.g. ZO-1, JAMA, Cld1, Cld3 and Ocl) and MUC2 expression, the latter is known to contribute to enhanced colonic mucosa structure. The improved gut barrier function in turn promotes a balanced luminal environment by which the colonic microbial community structure and activity are sustained. Collectively, findings of this study elucidated that PPE supplementation was a promising dietary approach against unhealthy dietary factors to lower the risk of inflammatory syndrome and associated obesity through interplaying with the gut and symbiotic microbiota. The low and high doses of the present study are equivalent to a daily intake of 75 g and 750 g fresh purple potato. Further research will focus on the molecular mechanisms of the observed activities, and interactions between polyphenols/anthocyanins or their metabolites and the microbiota.

Acknowledgments

We thank Dr. Zhanhui Lu of the Guelph Research & Development Centre, Agriculture & Agri-Food Canada (AAFC) for his assistance in statistical analysis. This project is supported by the A-Base Project (#J-002252.001.04) of AAFC.

Conflict of interest

The authors declare that they have no known competing financial interests or personal relationships that could have appeared to influence the work reported in this paper.

Author contributions

Hua Zhang: Methodology, overall experiments, data curation, original draft preparation; Ronghua Liu: Chromatography, lab protocols; Lili Mats: Metabolomics, data analysis; Dion Lepp: 16S rRNA gene sequencing, microbiota composition and data curation; Honghui Zhu: Mass spectrometry, data curation; Yuhuan Chen: Animal tissue collecting and processing; Shilian Zheng: Animal plasma and tissue processing and analysis; Yoshinori Mine: Animal protocols, review & editing; Rong Tsao: Conceptualization, funding acquisition, project administration, resources, supervision, writing-review & editing.

Supplementary material

Table S1. Composition of experimental foods (g/kg).

Table S2. Amplicon sequence variants (ASVs) affected by purple potato extract (PPE).

Figure S1. The impact of PPE on the gut sensing activity. The negative control (NC) group represents the mice that have a normal diet, while the HF/LPS and HF represent the mice administered with HFD with or without LPS. The mice pre-treated with PPE at low and high doses are designated LPP and HPP, respectively. Results are represented as mean ± SEM, n = 6. Values without a

common letter are significantly different at $p < 0.05$.

Figure S2. The modulatory effect of PPE on fecal microbial profile as demonstrated in the pathway of bile secretion. colored bile acid metabolites are the ones involved in the regulatory functions of bile secretion.

References

Alcock, J., Maley, C.C., and Aktipis, C.A. (2014). Is eating behavior manipulated by the gastrointestinal microbiota? Evolutionary pressures and potential mechanisms. Bioessays 36(10): 940–949.

Bolyen, E., Rideout, J.R., Dillon, M.R., Bokulich, N.A., Abnet, C.C., Al-Ghalith, G.A., Alexander, H., Alm, E.J., Arumugam, M., Asnicar, F., Bai, Y., Bisanz, J.E., Bittinger, K., Brejnrod, A., Brislawn, C.J., Brown, C.T., Callahan, B.J., Caraballo-Rodriguez, A.M., Chase, J., Cope, E.K., Da Silva, R., Diener, C., Dorrestein, P.C., Douglas, G.M., Durall, D.M., Duvallet, C., Edwardson, C.F., Ernst, M., Estaki, M., Fouquier, J., Gauglitz, J.M., Gibbons, S.M., Gibson, D.L., Gonzalez, A., Gorlick, K., Guo, J., Hillmann, B., Holmes, S., Holste, H., Huttenhower, C., Huttley, G.A., Janssen, S., Jarmusch, A.K., Jiang, L., Kaehler, B.D., Kang, K.B., Keefe, C.R., Keim, P., Kelley, S.T., Knights, D., Koester, I., Kosciolek, T., Kreps, J., Langille, M.G.I., Lee, J., Ley, R., Liu, Y.X., Loftfield, E., Lozupone, C., Maher, M., Marotz, C., Martin, B.D., McDonald, D., McIver, L.J., Melnik, A.V., Metcalf, J.L., Morgan, S.C., Morton, J.T., Naimey, A.T., Navas-Molina, J.A., Nothias, L.F., Orchanian, S.B., Pearson, T., Peoples, S.L., Petras, D., Preuss, M.L., Pruesse, E., Rasmussen, L.B., Rivers, A., Robeson, M.S. 2nd, Rosenthal, P., Segata, N., Shaffer, M., Shiffer, A., Sinha, R., Song, S.J., Spear, J.R., Swafford, A.D., Thompson, L.R., Torres, P.J., Trinh, P., Tripathi, A., Turnbaugh, P.J., Ul-Hasan, S., van der Hooft, J.J.J., Vargas, F., Vazquez-Baeza, Y., Vogtmann, E., von Hippel, M., Walters, W., Wan, Y., Wang, M., Warren, J., Weber, K.C., Williamson, C.H.D., Willis, A.D., Xu, Z.Z., Zaneveld, J.R., Zhang, Y., Zhu, Q., Knight, R., and Caporaso, J.G. (2019). Reproducible, interactive, scalable and extensible microbiome data science using QIIME 2. Nat. Biotechnol. 37(8): 852–857.

Cani, P.D. (2018). Human gut microbiome: hopes, threats and promises. Gut 67(9): 1716–1725.

Cardona, F., Andrés-Lacueva, C., Tulipani, S., Tinahones, F.J., and Queipo-Ortuño, M.I. (2013). Benefits of polyphenols on gut microbiota and implications in human health. J. Nutr. Biochem. 24(8): 1415–1422.

Castillo-Armengol, J., Fajas, L., and Lopez-Mejia, I.C. (2019). Inter-organ communication: a gatekeeper for metabolic health. EMBO Rep. 20(9): e47903.

Chu, H., and Mazmanian, S.K. (2013). Innate immune recognition of the microbiota promotes host-microbial symbiosis. Nat. Immunol. 14(7): 668.

Crosby, K., Simendinger, J., Grange, C., Ferrante, M., Bernier, T., and Stanen, C. Immunohistochemistry protocol for paraffin-embedded tissue section - advertisement. *Cell Signal Technol* 2016. Available at: https://www.jove.com/video/5064/immunohistochemistryprotocol-for-paraffin-embedded-tissue-sections.

Duan, Y., Zeng, L., Zheng, C., Song, B., Li, F., Kong, X., and Xu, K. (2018). Inflammatory Links Between High Fat Diets and Diseases. Front. Immunol. 9: 2649.

Fedarko, M.W., Martino, C., Morton, J.T., Gonzalez, A., Rahman, G., Marotz, C.A., Minich, J.J., Allen, E.E., and Knight, R. (2020). Visualizing'omic feature rankings and log-ratios using Qurro. NAR Genom. Bioinform. 2(2): lqaa023.

Fossen, T., Cabrita, L., and Andersen, O.M. (1998). Colour and stability of pure anthocyanins influenced by pH including the alkaline region. Food Chem. 63(4): 435–440.

Garrett, W.S., Gordon, J.I., and Glimcher, L.H. (2010). Homeostasis and inflammation in the intestine. Cell 140(6): 859–870.

Gibson, G.R., Probert, H.M., Van Loo, J., Rastall, R.A., and Roberfroid, M.B. (2004). Dietary modulation of the human colonic microbiota: updating the concept of prebiotics. Nutr. Res. Rev. 17(2): 259–275.

Gomes, J.M.G., de Assis Costa, J., and Alfenas, R.D.C.G. (2017). Metabolic endotoxemia and diabetes mellitus: a systematic review. Metabolism 68: 133–144.

Halfvarson, J., Brislawn, C.J., Lamendella, R., Vázquez-Baeza, Y., Walters, W.A., Bramer, L.M., D'Amato, M., Bonfiglio, F., McDonald, D., Gonzalez, A., McClure, E.E., Dunklebarger, M.F., Knight, R., and Jansson, J.K. (2017). Dynamics of the human gut microbiome in inflammatory bowel disease. Nat. Microbiol. 2(5): 17004.

Heyman-Linden, L., Kotowska, D., Sand, E., Bjursell, M., Plaza, M., Turner, C., Holm, C., Fak, F., and Berger, K. (2016). Lingonberries alter the gut microbiota and prevent low-grade inflammation in high-fat diet fed mice. Food Nutr. Res. 60: 29993.

Honda, A., Yoshida, T., Xu, G., Matsuzaki, Y., Fukushima, S., Tanaka, N., Doy, M., Shefer, S., and Salen, G. (2004). Significance of plasma 7α-hydroxy-4-cholesten-3-one and 27-hydroxycholesterol concentrations as markers for hepatic bile acid synthesis in cholesterol-fed rabbits. Metabolism 53(1): 42–48.

Hurst, R.D., Lyall, K.A., Wells, R.W., Sawyer, G.M., Lomiwes, D., Ngametua, N., and Hurst, S.M. (2020). Daily Consumption of an Anthocyanin-Rich Extract Made From New Zealand Blackcurrants for 5 Weeks Supports Exercise Recovery Through the Management of Oxidative Stress and Inflammation: A Randomized Placebo Controlled Pilot Study. Front. Nutr. 7: 16.

Joseph, S.V., Edirisinghe, I., and Burton-Freeman, B.M. (2014). Berries: anti-inflammatory effects in humans. J. Agric. Food Chem. 62(18): 3886–3903.

Khoo, H.E., Azlan, A., Tang, S.T., and Lim, S.M. (2017). Anthocyanidins and anthocyanins: colored pigments as food, pharmaceutical ingredients, and the potential health benefits. Food Nutr. Res. 61(1): 1361779.

Kotas, M.E., and Medzhitov, R. (2015). Homeostasis, inflammation, and disease susceptibility. Cell 160(5): 816–827.

Liu, H., Chen, X., Hu, X., Niu, H., Tian, R., Wang, H., Pang, H., Jiang, L., Qiu, B., Chen, X., Zhang, Y., Ma, Y., Tang, S., Li, H., Feng, S., Zhang, S., and Zhang, C. (2019). Alterations in the gut microbiome and metabolism with coronary artery disease severity. Microbiome 7(1): 68.

Livak, K.J., and Schmittgen, T.D. (2001). Analysis of relative gene expression data using real-time quantitative PCR and the 2− ΔΔCT method. methods 25(4): 402–408.

Martin, G., Kolida, S., Marchesi, J.R., Want, E., Sidaway, J.E., and Swann, J.R. (2018). In vitro modeling of bile acid processing by the human fecal microbiota. Front. Microbiol. 9: 1153.

Mehta, N.N., McGillicuddy, F.C., Anderson, P.D., Hinkle, C.C., Shah, R., Pruscino, L., Tabita-Martinez, J., Sellers, K.F., Rickels, M.R., and Reilly, M.P. (2010). Experimental endotoxemia induces adipose inflammation and insulin resistance in humans. Diabetes 59(1): 172–181.

Millet, S., Van Oeckel, M.J., Aluwe, M., Delezie, E., and De Brabander, D.L. (2010). Prediction of in vivo short-chain fatty acid production in hindgut fermenting mammals: problems and pitfalls. Crit. Rev. Food Sci. Nutr. 50(7): 605–619.

Moreira, A.P.B., Texeira, T.F.S., Ferreira, A.B., Peluzio, M.d.C.G., and Alfenas, R.d.C.G. (2012). Influence of a high-fat diet on gut microbiota, intestinal permeability and metabolic endotoxaemia. Br. J. Nutr. 108(5): 801–809.

Morton, J.T., Marotz, C., Washburne, A., Silverman, J., Zaramela, L.S., Edlund, A., Zengler, K., and Knight, R. (2019). Establishing microbial composition measurement standards with reference frames. Nat. Commun. 10(1): 2719.

Mosele, J.I., Gosalbes, M.J., Macia, A., Rubio, L., Vazquez-Castellanos, J.F., Jimenez Hernandez, N., Moya, A., Latorre, A., and Motilva, M.J. (2015). Effect of daily intake of pomegranate juice on fecal microbiota and feces metabolites from healthy volunteers. Mol. Nutr. Food Res. 59(10): 1942–1953.

Nair, A.B., and Jacob, S. (2016). A simple practice guide for dose conversion between animals and human. J. Basic. Clin. Pharm. 7(2): 27–31.

Nemes, A., Homoki, J.R., Kiss, R., Hegedus, C., Kovacs, D., Peitl, B., Gal, F., Stundl, L., Szilvassy, Z., and Remenyik, J. (2019). Effect of Anthocyanin-Rich Tart Cherry Extract on Inflammatory Mediators and Adipokines Involved in Type 2 Diabetes in a High Fat Diet Induced Obesity Mouse Model. Nutrients 11(9): 1966.

Nunez, M.F., and Magnuson, B.A. (2013). Anthocyanins in Health and Disease Prevention. In: Wallace, T.C. (Ed.). Anthocyanins in Health and Disease. CRC Press, Boca Raton, p. 1.

Parada Venegas, D., De la Fuente, M.K., Landskron, G., Gonzalez, M.J.,

Quera, R., Dijkstra, G., Harmsen, H.J.M., Faber, K.N., and Hermoso, M.A. (2019). Short Chain Fatty Acids (SCFAs)-Mediated Gut Epithelial and Immune Regulation and Its Relevance for Inflammatory Bowel Diseases. Front. Immunol. 10: 277.

Pendyala, S., Walker, J.M., and Holt, P.R. (2012). A high-fat diet is associated with endotoxemia that originates from the gut. Gastroenterology 142(5): 1100–1101.e1102.

Peterson, L.W., and Artis, D. (2014). Intestinal epithelial cells: regulators of barrier function and immune homeostasis. Nat. Rev. Immunol. 14(3): 141–153.

Power, K.A., Lepp, D., Zarepoor, L., Monk, J.M., Wu, W., Tsao, R., and Liu, R. (2016). Dietary flaxseed modulates the colonic microenvironment in healthy C57Bl/6 male mice which may alter susceptibility to gut-associated diseases. J. Nutr. Biochem. 28: 61–69.

Rios-Covian, D., González, S., Nogacka, A.M., Arboleya, S., Salazar, N., Gueimonde, M., and de los Reyes-Gavilán, C.G. (2020). An Overview on Fecal Branched Short-Chain Fatty Acids Along Human Life and as Related With Body Mass Index: Associated Dietary and Anthropometric Factors. Front. Microbiol. 11: 973.

Suganami, T., Nishida, J., and Ogawa, Y. (2005). A paracrine loop between adipocytes and macrophages aggravates inflammatory changes: role of free fatty acids and tumor necrosis factor alpha. Arterioscler Thromb. Vasc. Biol. 25(10): 2062–2068.

Tang, W.W., Li, D.Y., and Hazen, S.L. (2019). Dietary metabolism, the gut microbiome, and heart failure. Nat. Rev. Cardiol. 16(3): 137–154.

Tsuda, T. (2012). Dietary anthocyanin-rich plants: biochemical basis and recent progress in health benefits studies. Mol. Nutr. Food Res. 56(1): 159–170.

Vendrame, S., and Klimis-Zacas, D. (2015). Anti-inflammatory effect of anthocyanins via modulation of nuclear factor-κB and mitogen-activated protein kinase signaling cascades. Nutr. Rev. 73(6): 348–358.

Villena, J., and Kitazawa, H. (2014). Modulation of intestinal TLR4-inflammatory signaling pathways by probiotic microorganisms: lessons learned from Lactobacillus jensenii TL2937. Front. Immunol. 4: 512.

Wahlström, A., Sayin, S.I., Marschall, H.-U., and Bäckhed, F. (2016). Intestinal crosstalk between bile acids and microbiota and its impact on host metabolism. Cell Metab. 24(1): 41–50.

Ward, J.B.J., Lajczak, N.K., Kelly, O.B., O'Dwyer, A.M., Giddam, A.K., Ni Gabhann, J., Franco, P., Tambuwala, M.M., Jefferies, C.A., Keely, S., Roda, A., and Keely, S.J. (2017). Ursodeoxycholic acid and lithocholic acid exert anti-inflammatory actions in the colon. Am. J. Physiol. Gastrointest. Liver Physiol. 312(6): G550–G558.

Zeng, Y., Zhang, H., Zong, L., Tsao, R., Arie, H., Izumo, T., Shibata, H., and Mine, Y. (2019). Lactobacillus pentosus S-PT84 prevents LPS-induced low-grade chronic inflammation in a C57BL/6J mouse model. J. Funct. Foods 62: 103526.

Zhang, H., Hassan, Y.I., Renaud, J., Liu, R., Yang, C., Sun, Y., and Tsao, R. (2017). Bioaccessibility, bioavailability, and anti-inflammatory effects of anthocyanins from purple root vegetables using mono- and co-culture cell models. Mol. Nutr. Food Res. 61(10): 1600928.

Zhang, H., Hassan, Y.I., Renaud, J., Liu, R., Yang, C., Sun, Y., and Tsao, R. (2017). Bioaccessibility, bioavailability, and anti-inflammatory effects of anthocyanins from purple root vegetables using mono-and co-culture cell models. Mol. Nutr. Food Res. 61(10): 1600928.

Zhang, H., Kovacs-Nolan, J., Kodera, T., Eto, Y., and Mine, Y. (2015). gamma-Glutamyl cysteine and gamma-glutamyl valine inhibit TNF-alpha signaling in intestinal epithelial cells and reduce inflammation in a mouse model of colitis via allosteric activation of the calcium-sensing receptor. Biochim. Biophys. Acta 1852(5): 792–804.

Zhang, H., Liu, R., and Tsao, R. (2016). Anthocyanin-rich phenolic extracts of purple root vegetables inhibit pro-inflammatory cytokines induced by H2O2 and enhance antioxidant enzyme activities in Caco-2 cells. J. Funct. Foods 22: 363–375.

Zhang, H., Qi, R., Zeng, Y., Tsao, R., and Mine, Y. (2020). Chinese Sweet Leaf Tea (*Rubus suavissimus*) Mitigates LPS-Induced Low-Grade Chronic Inflammation and Reduces the Risk of Metabolic Disorders in a C57BL/6J Mouse Model. J. Agric. Food Chem. 68(1): 138–146.

Zhao, L., Yang, W., Chen, Y., Huang, F., Lu, L., Lin, C., Huang, T., Ning, Z., Zhai, L., Zhong, L.L., Lam, W., Yang, Z., Zhang, X., Cheng, C., Han, L., Qiu, Q., Shang, X., Huang, R., Xiao, H., Ren, Z., Chen, D., Sun, S., El-Nezami, H., Cai, Z., Lu, A., Fang, X., Jia, W., and Bian, Z. (2019). A Clostridia-rich microbiota enhances bile acid excretion in diarrhea-predominant irritable bowel syndrome. J. Clin. Invest. 130(1): 438–450.